

Available Energy and Ground States of Convective Hydrodynamic and Hydromagnetic Instabilities

Kaixuan Fan and Yao Zhou*

*School of Physics and Astronomy, Institute of Natural Sciences,
and MOE-LSC, Shanghai Jiao Tong University, Shanghai 200240, China*

(Dated: March 2, 2026)

We propose a method for predicting the nonlinear saturation level of convective instabilities in neutral and magnetized fluids. The method combines Gardner’s restacking algorithm, which computes the available energy and ground states of collisionless plasmas in phase space, and Lagrangian relaxation, where fluid elements find lower-energy equilibria while preserving local invariants. For the incompressible Rayleigh-Taylor instability, the problem is formally equivalent to Gardner’s and the restacking algorithm directly applies in configuration space. To treat compressibility, we follow restacking with Lagrangian relaxation to obtain the ground state, and the results show excellent agreement with direct numerical simulations. Successful extension to the $m = 0$ interchange instability in a Z-pinch demonstrates the method’s potential as a general framework for estimating the nonlinear extent of convective instabilities, which can facilitate the design and operation of fusion reactors.

Introduction—Convective instabilities are ubiquitous in fluids and plasmas, arising whenever an unfavorable stratification in an effective gravitational field allows elements to interchange and release potential energy [1]. In neutral fluids, a canonical example is the Rayleigh–Taylor instability (RTI), which drives rapid mixing and often dominates the nonlinear evolution in laboratory, geophysical, and astrophysical flows [2]. In magnetized plasmas, the closely related interchange and ballooning instabilities play an important role in setting confinement limits and mediating transport [3].

Linear stability is well described by the energy principle [4] and typically treated as a hard constraint on the design and operation of fusion reactors. Yet the nonlinear outcome of a linear instability can bifurcate between a major crash or benign saturation. In the tokamak core, the quasi-interchange instability can trigger sawteeth or maintain a helical steady-state [5–8]. In the periphery, the edge localized modes can induce intense heat pulses to the plasma facing components or manifest as small, “grassy” oscillations [9–11]. In stellarators, the β -limits predicted by linear stability theory tend to be soft, even though large-scale collapses still occur at times [12–14]. Despite significant theoretical efforts to characterize the nonlinear behaviors of these instabilities [15–18], a general framework remains elusive. In particular, a practical model that can efficiently estimate the nonlinear extent of the instabilities without invoking expensive simulations can expand the design and operation space of fusion reactors by relaxing linear stability constraints.

The available energy is a dynamics-agnostic nonlinear measure for kinetic instabilities in collisionless plasmas. The concept was introduced by Gardner [19] as the excess energy above a “ground state”, obtained by restacking incompressible phase-space elements to minimize energy. It was later formalized [20, 21] and successfully applied to

microinstabilities and the resulting turbulent transport in magnetic fusion plasmas [22–24], and also motivated studies of phase-space engineering [25, 26]. In meteorology, Lorenz [27] applied a similar approach to circulation in stratified air, defining the available potential energy with regard to a reference state—a stable equilibrium accessible by adiabatically rearranging fluid parcels. In more general settings, the reference state is calculated by minimizing energy using optimization algorithms [28–32], while an efficient and robust method remains elusive. A closely related idea is Lagrangian relaxation, where fluid elements rearrange to find energy-minimizing equilibria while preserving local invariants including mass, entropy, and magnetic flux [33–36]. Its solution is given in terms of a continuous configuration map, which is more restrictive than Gardner’s discontinuous restacking operation and hence cannot capture nonlinear convection alone.

In this letter, we present a novel restacking–relaxation method for calculating the available energy and ground states of convective instabilities by combining Gardner’s restacking and Lagrangian relaxation. We first show that the incompressible RTI admits an equivalent restacking formulation in configuration space. We then introduce a compressible extension by following restacking with Lagrangian relaxation to obtain the ground state, and verify the predictions against direct numerical simulations. Finally, we apply the method to the $m = 0$ (m being the poloidal mode number) interchange instability in a Z-pinch (i.e., sausage instability), which demonstrates its potential as a general framework for quantifying the nonlinear extent of macroscopic events in fusion plasmas.

Incompressible RTI—In collisionless plasmas, the governing Vlasov equation is a continuity equation in phase space $\mathbf{z} \equiv (\mathbf{x}, \mathbf{v})$. The flow is incompressible such that the volume $d\Gamma$ and the number density f associated with an arbitrary phase-space element is invariant as it moves. Subject to this constraint, Gardner defines the ground state as one that minimizes the energy $W = \int f\epsilon d\Gamma$, where the particle energy ϵ is a function of \mathbf{z} only [19].

* yao.zhou@sjtu.edu.cn

It follows that the ground state f_g is a monotonically decreasing function of ϵ , which can be obtained by restacking the incompressible phase-space elements, or formally, solving the following integrodifferential equation [20–23]:

$$\frac{df_g}{d\eta} = -\frac{\int \delta[\eta - \epsilon(\mathbf{z})] d\Gamma}{\int \delta[f_0(\mathbf{z}) - f_g] d\Gamma}, \quad (1)$$

where f_0 is the initial distribution function that may be unstable and $\delta(x)$ is the Dirac delta function. The available energy $A = W_0 - W_g$ provides a nonlinear bound on the magnitude of the instability.

We identify a configuration-space equivalency for incompressible fluids in an external gravitational field $\phi(\mathbf{x})$, similar to the incompressible variation of Lorenz’s theory [37, 38]. The continuity equation ensures that the mass density ρ associated with an arbitrary fluid element is invariant along with its volume dV . Subject to this constraint, the ground state ρ_g minimizes the energy $W = \int \rho\phi dV$ by restacking the incompressible fluid elements, such that ρ_g is a monotonically decreasing function of ϕ and

$$\frac{d\rho_g}{d\psi} = -\frac{\int \delta[\psi - \phi(\mathbf{x})] dV}{\int \delta[\rho_0(\mathbf{x}) - \rho_g] dV}, \quad (2)$$

where ρ_0 is the initial density distribution that may be unstable to RTI. The limitation of this analogy is that incompressibility is merely an approximation for fluids and plasmas. Next, we propose a compressible extension, and verify the incompressible case as a limit.

Compressible RTI—Similar to Lorenz [27], we seek a ground state that is a stable equilibrium and preserves all the local invariants of the initial state. In compressible fluids, the continuity equation still holds. The volume and the mass density of a co-moving fluid element are not invariant, but the mass ρdV is invariant. Meanwhile, the adiabatic equation implies that the specific entropy [$s = \ln(p/\rho^\gamma)$ in an ideal gas, where p is the pressure and γ the adiabatic index] is also invariant. These invariants now constrain the restacking process. For simplicity, we consider $\phi = gx$ with a positive constant g in Cartesian geometry. The initial density $\rho_0(x_0)$ and pressure $p_0(x_0)$ profiles are in force balance:

$$\rho_0 g + dp_0/dx_0 = 0. \quad (3)$$

As illustrated in Fig. 1(a), we find the ground state in two steps, the first being a discontinuous restacking operation. In this case, it is convenient to consider discrete fluid elements with the same volume and the restacking is still incompressible. That is, when an element initially at x_0 is moved to x_1 , its density and pressure are maintained so that $\rho_1 = \rho_0$, $p_1 = p_0$. To achieve stability, we restack the fluid elements to satisfy the Schwarzschild criterion, $ds/dx > 0$, a necessary and sufficient condition for linear stability [39]. Since s is invariant, similar to Eqs. (1) and (2), the restacked state is formally given by

$$\frac{ds_1}{dx_1} = \frac{1}{\int \delta[s_0(x_0) - s_1] dx_0}, \quad (4)$$

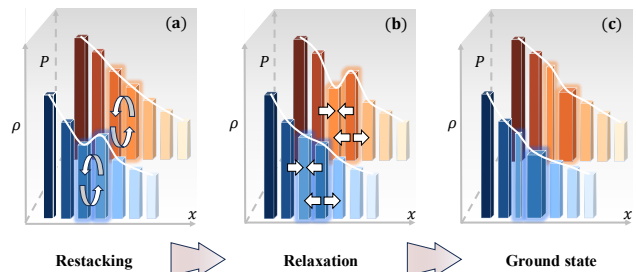


FIG. 1. A schematic of the restacking-relaxation method applied to the compressible RTI: (a) the unstable initial profiles subject to incompressible restacking; (b) the restacked profiles subject to Lagrangian relaxation; (c) the relaxed profiles, i.e., the ground state. The bars represent discrete fluid elements, whose colors denote the initial position x_0 .

where $s_0(x_0)$ and $s_1(x_1)$ denote the initial and restacked specific entropy profiles, respectively. In Fig. 2(a-c), we show an example of the restacked profiles $\rho_1(x_1)$, $p_1(x_1)$, and $s_1(x_1)$ (triangles) to compare with the unstable initial profiles (stars).

Unlike the incompressible case where the pressure is a gauge, here the restacked state is not in force balance. To further obtain an equilibrium state with lower energy, we adopt Lagrangian relaxation as illustrated in Fig. 1(b). Specifically, the fluid motion is governed by a continuous mapping $x_g(x_1)$, and the invariance of mass and entropy implies that [33]

$$\rho_g[x_g(x_1)] = \rho_1/J, \quad p_g[x_g(x_1)] = p_1/J^\gamma, \quad (5)$$

where the Jacobian $J(x_1) = dx_g/dx_1$ captures the compressibility of the fluid. Minimizing the potential energy $W = \int [\rho_g x_g g + p_g/(\gamma - 1)] dx_g$ yields the relaxed state as portrayed in Fig. 1(c), which satisfies force balance:

$$\rho_1(x_1)g + \frac{d}{dx_1} \left[\frac{p_1(x_1)}{J^\gamma} \right] = 0. \quad (6)$$

The equilibrium is stable for preserving the monotonicity of the specific entropy, $ds_g/dx_g = J^{-1}ds_1/dx_1 > 0$. We regard this invariants-preserving stable equilibrium as the ground state, based on which the available energy can be calculated. The corresponding profiles $\rho_g(x_g)$ and $p_g(x_g)$ in Fig. 2(a-c) (circles) show significant deviation from the restacked state to reach force balance.

To verify the method’s predictions, we perform direct numerical simulations using the *DedaLus* framework [40]. We solve the compressible fluid equations in 2D slab geometry (x, y) . The boundary conditions are periodic in y , and Neumann for the pressure and density and free-slip for the velocity field in x . Small hyper-diffusivities are included in the continuity and adiabatic equations for numerical stability. A large viscosity is used to damp out the RTI-driven flows so that the system settles to a near-equilibrium state. The gray broken curves in Fig. 3(a-b) show the initial conditions based on the globally unstable profiles in Fig. 2(a-b) (triangles), with the maximum

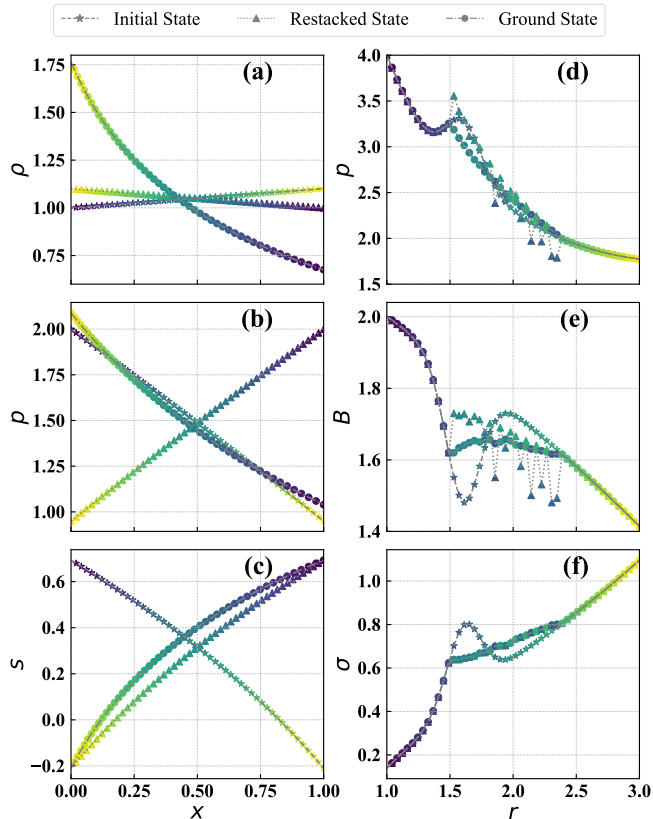


FIG. 2. Examples of initial (stars), restacked (triangles), and ground state (circles) profiles: the density (a), pressure (b), and specific entropy (c) in the compressible RTI; and the pressure (d), magnetic field (e), and stability indicator σ (f) in the sausage instability. The markers represent discrete fluid elements, whose colors denote the initial position (x_0 or r_0).

pressure P_0 varied to adjust compressibility. The detailed settings can be found in the Supplemental Material.

In Fig. 3(a-b), all the settled profiles (solid) show excellent agreement with the respective ground-state profiles (broken) obtained with the proposed method, corroborating that the latter are consistent with the constrained energy-minimizing equilibria. This naturally translates to the agreement between the decayed potential energy (triangles) in the simulations and the calculated available energy shown in Fig. 3(c). In particular, the most compressible case ($P_0 = 2$) corresponds to Fig. 2(a-b), and the least compressible case ($P_0 = 10$) approaches the incompressible limit. Also, we perform simulations with zero viscosity and a small hyper-viscosity and measure the peak (stars) kinetic energy. In Fig. 3(c), both quantities are found to be proportional to the available energy, further verifying its effectiveness as a metric for the nonlinear extent of the RTI.

Sausage Instability—By combining Gardner’s restacking and Lagrangian relaxation, we can achieve the ground state robustly and efficiently in a general setting, irrespective of the specific geometry or types of local invari-

ants. We use the sausage instability as an example to show how to treat magnetized fluids and more complex geometry. It is an axisymmetric ($m = 0$) interchange mode in a Z-pinch, which features a purely poloidal magnetic field $\mathbf{B} = B\hat{\theta}$ in cylindrical geometry (r, θ, z). The initial profiles $p_0(r_0)$ and $B_0(r_0)$ are in force balance:

$$\frac{d}{dr_0} \left(p_0 + \frac{B_0^2}{2} \right) + \frac{B_0^2}{r_0} = 0. \quad (7)$$

In ideal magnetohydrodynamics (MHD), the magnetic flux $\mathbf{B} \cdot d\mathbf{S}$ through a co-moving area element $d\mathbf{S}$ is invariant [33]. In our case, this entails that $B_1 dr_1 = B_0 dr_0$ when an element is radially restacked from r_0 to r_1 .

Similar to the RTI case, we resort to the linear stability criterion [41] for a restacking strategy:

$$\frac{2\gamma B^2}{\gamma p + B^2} + \frac{r}{p} \frac{dp}{dr} > 0. \quad (8)$$

This necessary and sufficient condition can be written in a form similar to the Schwarzschild criterion:

$$\frac{d\sigma}{dr} > 0, \quad \sigma = \ln \left(\frac{rp^{1/\gamma}}{B} \right). \quad (9)$$

One can prove that σ is also invariant based on the invariance of mass, entropy, and magnetic flux, so that we can restack the fluid elements according to Eq. (9).

Here, we can consider discrete elements with the same volume $dV \sim r dr$, so that the restacking operation is incompressible. In this case, we have $B_1/r_1 = B_0/r_0$ and $p_1 = p_0$, and the restacked state is formally given by

$$\frac{d\sigma_1}{dr_1} = \frac{r_1}{\int \delta[\sigma_0(r_0) - \sigma_1] r_0 dr_0}. \quad (10)$$

Alternatively, we can consider discrete elements with the same radial extent dr , so that the restacking operation is “equidistant”. In this case, we have $p_1/r_1^\gamma = p_0/r_0^\gamma$ and $B_1 = B_0$, and the restacked state is formally given by

$$\frac{d\sigma_1}{dr_1} = \frac{1}{\int \delta[\sigma_0(r_0) - \sigma_1] dr_0}. \quad (11)$$

The restacked states in the two cases will have different profiles but the same order of fluid elements by ascending σ , so the ground states then obtained with Lagrangian relaxation will be the same (c.f. Supplemental Material). Similar to Eq. (6), the equilibrium that minimizes the potential energy $W = \int [B_g^2/2 + p_g/(\gamma - 1)] r_g dr_g$ reads

$$\frac{d}{dr_1} \left(\frac{p_1}{J^\gamma} + \frac{r_g^2 B_1^2}{r_1^2 2J} \right) + \frac{B_1^2}{r_1 J} = 0, \quad (12)$$

where $J = (r_g/r_1)(dr_g/dr_1)$ now includes metric factors. The solution $r_g(r_1)$ then yields the ground state profiles

$$B_g[r_g(r_1)] = r_g B_1 / r_1 J, \quad p_g[r_g(r_1)] = p_1 / J^\gamma. \quad (13)$$

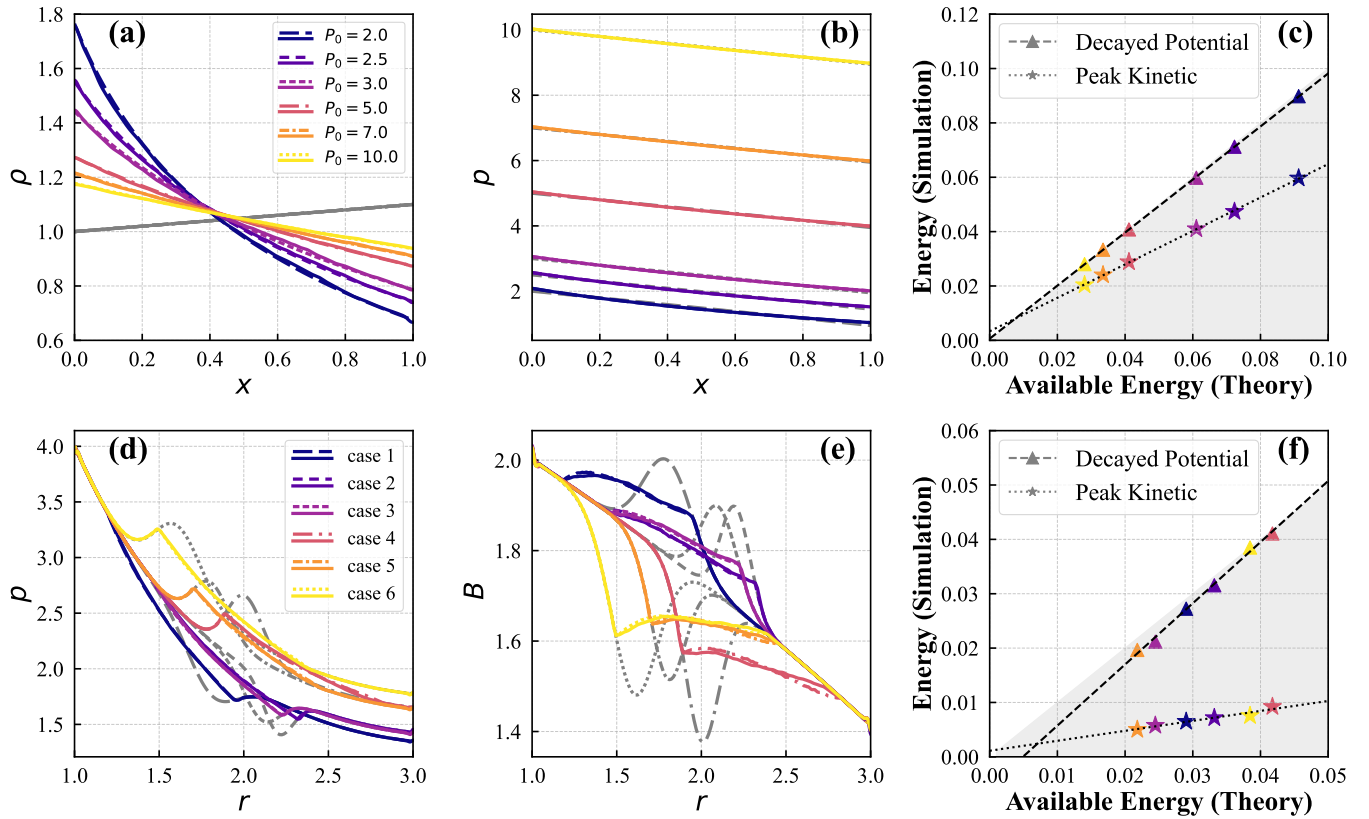


FIG. 3. Comparison between the ground states (broken colored) obtained with the proposed method and the settled profiles (solid colored) in viscous simulations: density (a) and pressure (b) profiles in the RTI, and pressure (d) and magnetic field (e) for the sausage instability. The gray broken lines show the initial profiles. The decayed potential energy in viscous simulations (triangles) and the peak kinetic energy in non-viscous simulations (stars) all show proportionality to the available energy for both the RTI (c) and the sausage instability (f). The black broken lines show linear fits.

An example of the initial (stars), restacked (triangles, obtained with equidistant restacking), and ground state (circles) profiles is presented in Fig. 2(d-f). The initial profiles feature a locally unstable pressure hump, unlike the globally unstable profiles in Fig. 2(a-c). The profiles' non-monotonicity results in the non-smoothness of the restacked profile, which highlights the discontinuous nature of the restacking operation. The non-smoothness is mitigated by Lagrangian relaxation in the ground state, and does not have a significant impact on the calculation of the available energy.

To verify the predictions, we solve the ideal MHD equations in axisymmetric cylindrical geometry (r, z) using *Dedalus*. The simulation settings are similar to those for the RTI (see Supplemental Material for details). The position and shape of the pressure hump (and hollow) are varied in the initial profiles (gray broken) shown in Fig.3(d-e), with case 6 corresponding to Fig. 2(d-e). In all cases the settled profiles (solid) in the simulations agree well with the ground states (colored broken) predicted. In Fig.3(f), the decayed potential energy in viscous simulations and the peak kinetic energy in non-viscous simulations all show clear proportionality to the available energy. The agreement is less perfect than the globally

unstable RTI cases in Fig.3(c) because here the available energy takes up a much smaller fraction of the total energy, so that the results are more sensitive to numerical settings, etc. Nevertheless, the trend remains obvious.

Discussion—In this work, we present a method for calculating the available energy as a metric for the nonlinear extent of convective hydrodynamic and hydromagnetic instabilities. The method extends Gardner's restacking algorithm to configuration space, followed by Lagrangian relaxation to treat compressibility. Its effectiveness is demonstrated by successful application to the RTI and the sausage instability. Future work should consider more complicated instabilities in realistic geometries, such as interchange modes in a screw pinch and ultimately ballooning modes in toroidal plasmas.

The examples presented above enjoy two conveniences that simplify the restacking process but may not exist in general. One is an explicit local necessary and sufficient stability criterion, and the other is that the criterion can be expressed in terms of a local invariant. For the former, note that the restacking strategy does not require a necessary and sufficient criterion. In fact, in Gardner's restacking algorithm, $df_g/d\epsilon < 0$ is only a sufficient condition for stability. (The necessary and sufficient condition is given

by Penrose [42].) In the Supplemental Material, we show an example where restacking based on a necessary (but not sufficient) criterion is still effective. When the latter does not apply, the restacked state may not be obtained directly, and the relaxed state may become unstable. In this case, one can apply the restacking-relaxation method iteratively to obtain the ground state.

Acknowledgments—The authors are grateful for useful discussions with Drs. Q. Sun, H. Zhu, X. Xu, X. Wu, and G. Jia. This research is supported by the National MCF R&D Program under Grant Number 2024YFE03230400, the National Natural Science Foundation of China under Grant Number 12305246, and the Fundamental Research Funds for the Central Universities.

-
- [1] S. Chandrasekhar, *Hydrodynamic and hydromagnetic stability* (Courier Corporation, 2013).
- [2] Y. Zhou, Rayleigh–Taylor and Richtmyer–Meshkov instability induced flow, turbulence, and mixing. I, *Physics Reports* **720–722**, 1 (2017).
- [3] J. P. Freidberg, *Ideal MHD* (Cambridge University Press, 2014).
- [4] I. B. Bernstein, E. A. Frieman, M. D. Kruskal, and R. M. Kulsrud, An energy principle for hydromagnetic stability problems, *Proceedings of the Royal Society of London. Series A. Mathematical and Physical Sciences* **244**, 17 (1958).
- [5] J. A. Wesson, Sawtooth oscillations, *Plasma Physics and Controlled Fusion* **28**, 243 (1986).
- [6] J. E. Menard, R. E. Bell, D. A. Gates, S. M. Kaye, B. P. LeBlanc, F. M. Levinton, S. S. Medley, S. A. Sabbagh, D. Stutman, K. Tritz, and H. Yuh, Observation of instability-induced current redistribution in a spherical-torus plasma, *Physical Review Letters* **97**, 095002 (2006).
- [7] S. C. Jardin, N. Ferraro, and I. Krebs, Self-organized stationary states of tokamaks, *Physical Review Letters* **115**, 215001 (2015).
- [8] S. C. Jardin, I. Krebs, and N. Ferraro, A new explanation of the sawtooth phenomena in tokamaks, *Physics of Plasmas* **27**, 032509 (2020).
- [9] H. Zohm, Edge localized modes (ELMs), *Plasma Physics and Controlled Fusion* **38**, 105 (1996).
- [10] A. Kirk, B. Koch, R. Scannell, H. R. Wilson, G. Counsell, J. Dowling, A. Herrmann, R. Martin, and M. Walsh, Evolution of filament structures during edge-localized modes in the mast tokamak, *Physical Review Letters* **96**, 185001 (2006).
- [11] G. S. Xu, Q. Q. Yang, N. Yan, Y. F. Wang, X. Q. Xu, H. Y. Guo, R. Maingi, L. Wang, J. P. Qian, X. Z. Gong, V. S. Chan, T. Zhang, Q. Zang, Y. Y. Li, L. Zhang, G. H. Hu, and B. N. Wan, Promising high-confinement regime for steady-state fusion, *Physical Review Letters* **122**, 255001 (2019).
- [12] A. Weller, S. Sakakibara, K. Y. Watanabe, K. Toi, J. Geiger, M. C. Zarnstorff, S. R. Hudson, A. Reiman, A. Werner, C. Nührenberg, S. Ohdachi, Y. Suzuki, and H. Yamada, Significance of MHD Effects in Stellarator Confinement, *Fusion Science and Technology* **50**, 158 (2006).
- [13] S. Ohdachi, K. Watanabe, K. Tanaka, Y. Suzuki, Y. Takemura, S. Sakakibara, X. Du, T. Bando, Y. Narushima, R. Sakamoto, J. Miyazawa, G. Motojima, and T. Morisaki, Observation of the ballooning mode that limits the operation space of the high-density super-dense-core plasma in the LHD, *Nuclear Fusion* **57**, 066042 (2017).
- [14] Y. Zhou, K. Aleynikova, C. Liu, and N. M. Ferraro, benign saturation of ideal ballooning instability in a high-performance stellarator, *Physical Review Letters* **133**, 135102 (2024).
- [15] H. Wilson and S. Cowley, Theory for explosive ideal magnetohydrodynamic instabilities in plasmas, *Physical Review Letters* **92**, 175006 (2004).
- [16] P. Zhu, C. C. Hegna, and C. R. Sovinec, Exponential growth of nonlinear ballooning instability, *Physical Review Letters* **102**, 235003 (2009).
- [17] P. W. Xi, X. Q. Xu, and P. H. Diamond, Phase dynamics criterion for fast relaxation of high-confinement-mode plasmas, *Physical Review Letters* **112**, 085001 (2014).
- [18] C. J. Ham, S. C. Cowley, G. Brochard, and H. R. Wilson, Nonlinear stability and saturation of ballooning modes in tokamaks, *Physical Review Letters* **116**, 235001 (2016).
- [19] C. S. Gardner, Bound on the energy available from a plasma, *Physics of Fluids* **6**, 839 (1963).
- [20] I. Y. Dodin and N. Fisch, Variational formulation of the Gardner’s restacking algorithm, *Physics Letters A* **341**, 187 (2005).
- [21] P. Helander, Available energy and ground states of collisionless plasmas, *Journal of Plasma Physics* **83**, 715830401 (2017).
- [22] P. Helander, Available energy of magnetically confined plasmas, *Journal of Plasma Physics* **86**, 905860201 (2020).
- [23] R. Mackenbach, J. H. Proll, and P. Helander, Available energy of trapped electrons and its relation to turbulent transport, *Physical Review Letters* **128**, 175001 (2022).
- [24] R. Mackenbach, P. Helander, M. Landreman, S. Brunner, and J. Proll, On the curvature-driven ion-temperature-gradient instability and its available energy, *Journal of Plasma Physics* **91**, E144 (2025).
- [25] E. J. Kolmes and N. J. Fisch, Upper and lower bounds on phase-space rearrangements, *Physics of Plasmas* **31**, 042109 (2024).
- [26] H. Qin, E. J. Kolmes, M. Updike, N. Bohlsen, and N. J. Fisch, Gromov ground state in phase space engineering for fusion energy, *Phys. Rev. E* **111**, 025205 (2025).
- [27] E. N. Lorenz, Available potential energy and the maintenance of the general circulation, *Tellus A: Dynamic Meteorology and Oceanography* **7**, 157 (1955).
- [28] E. N. Lorenz, Numerical evaluation of moist available energy, *Tellus* **31**, 230 (1979).
- [29] M. Hieronymus and J. Nycander, Finding the minimum potential energy state by adiabatic parcel rearrangements with a nonlinear equation of state: An exact solution in polynomial time, *Journal of Physical Oceanography* **45**, 1843 (2015).
- [30] E. M. Stansifer, P. A. O’Gorman, and J. I. Holt, Accurate computation of moist available potential energy with the munkres algorithm, *Quarterly Journal of the Royal*

- Meteorological Society **143**, 288 (2017).
- [31] B. L. Harris and R. Tailleux, Assessment of algorithms for computing moist available potential energy, Quarterly Journal of the Royal Meteorological Society **144**, 1501 (2018).
- [32] D. Hosking, D. Wasserman, and S. Cowley, Metastability of stratified magnetohydrostatic equilibria and their relaxation, Journal of Plasma Physics **91**, E35 (2025).
- [33] W. A. Newcomb, Lagrangian and Hamiltonian Methods in Magnetohydrodynamics, Nuclear Fusion: Supplement, part 2 **2**, 451 (1962).
- [34] I. J. D. Craig and A. D. Sneyd, A dynamic relaxation technique for determining the structure and stability of coronal magnetic fields, The Astrophysical Journal **311**, 451 (1986).
- [35] S. Candelaresi, D. Pontin, and G. Hornig, Mimetic Methods for Lagrangian Relaxation of Magnetic Fields, SIAM Journal on Scientific Computing **36**, B952 (2014).
- [36] Y. Zhou, H. Qin, J. W. Burby, and A. Bhattacharjee, Variational integration for ideal magnetohydrodynamics with built-in advection equations, Physics of Plasmas **21**, 102109 (2014).
- [37] D. Holliday and M. E. McIntyre, On potential energy density in an incompressible, stratified fluid, Journal of Fluid Mechanics **107**, 221 (1981).
- [38] K. B. Winters, P. N. Lombard, J. J. Riley, and E. A. D’Asaro, Available potential energy and mixing in density-stratified fluids, Journal of Fluid Mechanics **289**, 115 (1995).
- [39] H. Kull, Theory of the Rayleigh-Taylor instability, Physics Reports **206**, 197 (1991).
- [40] K. J. Burns, G. M. Vasil, J. S. Oishi, D. Lecoanet, and B. P. Brown, Dedalus: A flexible framework for numerical simulations with spectral methods, Physical Review Research **2**, 023068 (2020).
- [41] B. Kadomtsev *et al.*, Hydromagnetic stability of a plasma, Reviews of plasma physics **2**, 153 (1966).
- [42] O. Penrose, Electrostatic instabilities of a uniform non-maxwellian plasma, Physics of Fluids **3**, 258 (1960).